Frontiers in Bioscience Landmark

Front. Biosci. (Landmark Ed) **2022**; 27(1): 028
http://doi.org/10.31083/j.fbl2701028

Original Research

A rhodamine derivative probe for highly selective detection of Cu(II)

Liming Hu[1], Yifan Lin[1], Peng Wang[1], Hongsheng Zhang[1], Minyao Liu[1], Shanyan Mo[1,*]

[1]College of Life Science and Chemistry, Beijing Key Laboratory of Environmental and Oncology, Faculty of Environment and Life, Beijing University of Technology, 100124 Beijing, China
*Correspondence: mo@bjut.edu.cn (Shanyan Mo)
Academic Editor: Anna Lewinska
Submitted: 18 May 2021 Revised: 5 July 2021 Accepted: 16 July 2021 Published: 18 January 2022

Abstract

Background: Abnormal Cu(II) ions levels may affect many biological functions, and it is of great importance to detect Cu(II) ions in organisms. **Methods**: Herein, we report a near-infrared (NIR) fluorescent probe **EtRh-N-NH$_2$** for the detection of Cu(II). In the probe structure, a rhodamine core was used, and a hydrazine group was employed as the responsive site. **Results & Conlusions**: **EtRh-N-NH$_2$** displayed sensitive, specific and fast response upon Cu(II) with excellent linear relationship between the concentration and fluorescence emission intensity in 0–1 μM range. The releasing **EtRh-COOH** exhibited 762 nm of emission wavelength with a 75 nm of Stokes shift.

Keywords: Large Stokes shift; Cu(II) detection; Fluorescent probe

1. Introduction

The copper element amount in the human body and other biological systems is only trace but essential and indispensable [1,2]. In organisms, copper, existing as an oxidation state Cu(II), participates in many important redox reactions [3]. The Cu(II) concentration should maintain at a certain range of about 40 μg L^{-1} to meet the normal metabolism of organisms in the human body [4]. Excessive Cu(II) concentration can cause gastrointestinal dysfunction or liver and kidney damage. But on the other hand deficient Cu(II) concentration can cause a variety of neurodegenerative diseases [5,6]. Therefore, it is significant to develop a reliable method to monitor Cu(II) in the complex organisms.

The traditional techniques based on inductively coupled plasma (ICP) method (including atomic absorption spectroscopy (AAS) [7], atomic emission spectroscopy (AES) [8], and mass spectrometry (MS) [9]) could detect Cu(II) ions concentration in high accuracy; however, it is difficult to monitor the Cu(II) compounds in real-time and in the biological system using these ICP methods [10]. There are lots of methods for the detection of copper ions, mainly including fluorescent hybrid nanomaterials [11] and fluorescent chemical sensors [12]. Emerging fluorescent hybrid nanomaterials includes quantum dots (QDs), metal nanoclusters (NCs), carbon dots (CDs), MXenes and polymer nanoparticles (NPs) [13,14]. Fluorescence chemical sensors are mostly based on the following types: deoxyribonucleic acid [15], fluorophores [16,17], metal-organic framework (MOF) [18], copolymers [19], Schiff bases [20], and silica nanoparticles [21]. Among them, chemical sensors containing fluorophores have attracted much attention. By introducing various ligands and fluorophores, such as fluorescein, rhodamine, naphthalimide and boron dipyrromethene (BODIPY), the selective detection of metal ions can be successfully achieved. The process involves different sensing mechanisms including photo-induced electron transfer (PET), fluorescence resonance energy transfer (FRET), intramolecular charge transfer (ICT), chelation enhanced fluorescence (CHEF), excited state intramolecular proton transfer (ESIPT) and Aggregation induced emission (AIE). Compared with nanomaterials, organic chemical probes are of superior biocompatibility, flexible structural modification and relatively low toxicity. In addition, fluorescence bioimaging technology allows us to detect a variety of metal ions including Cu(II) *in vivo* at a subcellular level [22,23], thus they were receiving much more attention.

Cu(II) fluorescent chemical sensors are mostly designed and synthesized based on inorganic [rhenium (I), ruthenium (II), iridium (III), zinc (II), and gold (I)] [24] and organic materials [25]. And these probes can be classified into two categories based on their mechanism of the fluorescence production [26,27]. The first ones produce fluorescence via the coordination with the Cu(II) ions; however, the fluorescence is generally weak due to the heavy atom effect and the low efficiency of photoinduced electron transfer (PET) process. Secondly, organic material chemical sensors are designed by the fluorescence technology of organic small molecules to sense metal ions. Through the complexation of ligands and metallic copper, it can produce spectral shifts, binding/association/dissociation constants, and color changes to achieve the sensing effect of Cu(II). The second category of Cu(II) detection probes produce fluorescence after the response with Cu(II) ions. Before the response, little fluorescence was emissive; thus, image with higher signal to background ratio can be achieved. Because of its instant response, high sensitivity and selectivity, easy measurement and real-time monitoring, fluorescent sensors based on organic materials have received extensive attention [28].

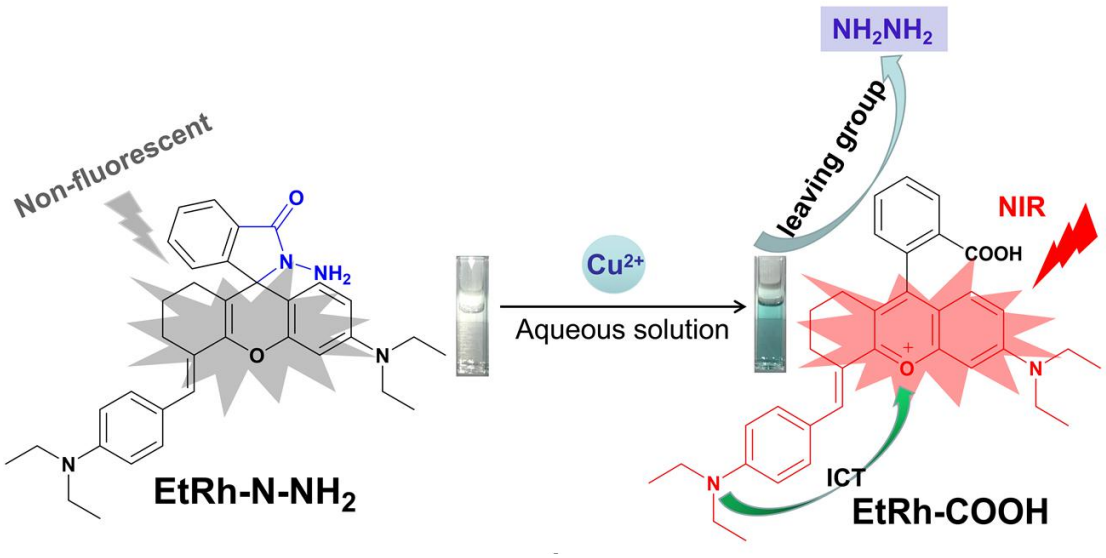

Scheme 1. Mechanistic proposal of the response of EtRh-N-NH_2 upon treatment with Cu(II).

Among the NIR dyes, rhodamine derivatives [29–32] are widely used as responsive fluorescent probes by their characteristic spirolactam ring-opening and -closing process (**Supplementary Table 1**). More importantly, the rhodamines are of high fluorescence quantum yield, large molar extinction coefficient, good stability upon photo irradiation, and easy structural modification. However, many reported rhodamines and their derivatives used for Cu(II) detection exhibited short fluorescence emission wavelength (mostly less than 600 nm), and probes with emission in the NIR range (600–900 nm) are more advantageous because of their better tissue penetration depth [33–35]. Besides, the Stokes shifts of the reported dyes are usually small (less than 50 nm), leading to a severe autofluorescence issue in fluorescence imaging [36]. Herein, we designed a new rhodamine-based near-infrared probe **EtRh-N-NH_2** acting as a turn-on chemo-sensor for Cu(II) with a spirocyclic hydrazide group as the Cu(II) recognition group [37,38]. The probe **EtRh-N-NH_2** shows negligible fluorescence. However, upon the treatment with Cu(II) compound, the hydrazide group was hydrolyzed to generate a ring-opened dye **EtRh-COOH** with extremely strong fluorescence signals at 762 nm. Thus, the Cu(II) compound turns on the fluorescence (Scheme 1). Meanwhile, it is indicated from the results that the response is highly specific for Cu(II) compound. In the aspect of analytical chemistry, within the range of 0–1.0 μM, the response shows an excellent linear relationship with the $R^2 = 0.997$. Besides, the detection limit is only 6 nM. In addition, the Stokes shift of the probe is as large as 75 nm. Finally, the probe reveals its ability to detect various active substances *in vitro*.

2. Results and discussion

2.1 Synthesis of EtRh-N-NH_2

As described, **EtRh-N-NH_2** was synthesized via a three-step method from 2-(5-(diethylamino)-2-hydroxybenzoyl) benzoic acid (Scheme 2). At first, the reaction of compound **1** and cyclohexanone generates the three-membered ring intermediate **2** in the presence of concentrated sulfuric acid. Then the afforded **2** was condensed with 4-diethylaminobenzaldehyde to give raise to the fluorophore **EtRh-COOH**. Finally, the carboxyl part of the fluorophore underwent a ring-closure reaction to obtain the desired aminohydrazide probe **EtRh-N-NH_2**.

2.2 Mechanistic study of the response

As depicted in Scheme 3, we proposed the mechanism of the fluorescent turning-on process of the designed probe **EtRh-N-NH_2**. The Cu(II) powerfully bonds and chelates with the amino and carbonyl groups of the probe, leading to the hydrolysis of the hydrazide and formation of the strong fluorescent **EtRh-COOH**. Eventually, the fluorescence is turned on.

To validate the mechanism, we performed the HPLC experiments. As shown in Fig. 1, the retention times for **EtRh-COOH** and **EtRh-N-NH_2** were 3.20 min and 4.38 min, respectively. Upon adding Cu(II) compounds, the peak of **EtRh-N-NH_2** disappeared gradually; meanwhile, the peak of **EtRh-COOH** raised proportionately, suggesting the generation of **EtRh-COOH**. In addition, the high-resolution detection of the mixed solution of the probe **EtRh-N-NH_2** and Cu(II) compounds can simultaneously obtain the mass spectrum peaks of **EtRh-N-NH_2** and **EtRh-COOH** (**Supplementary Fig. 1**). Therefore, we proved the reaction mechanism in Scheme 3.

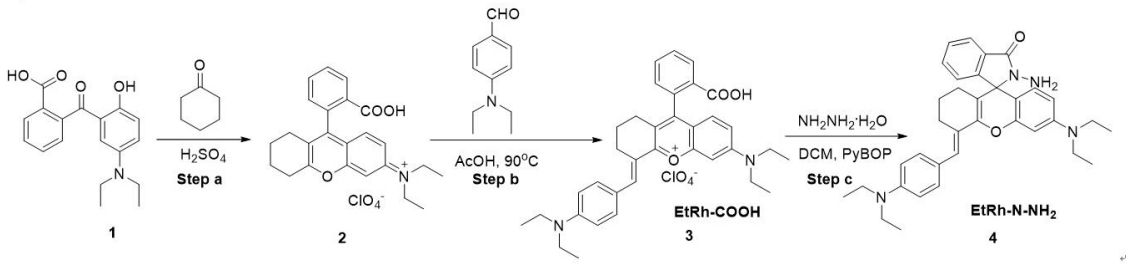

Scheme 2. Synthesis of EtRh-N-NH_2.

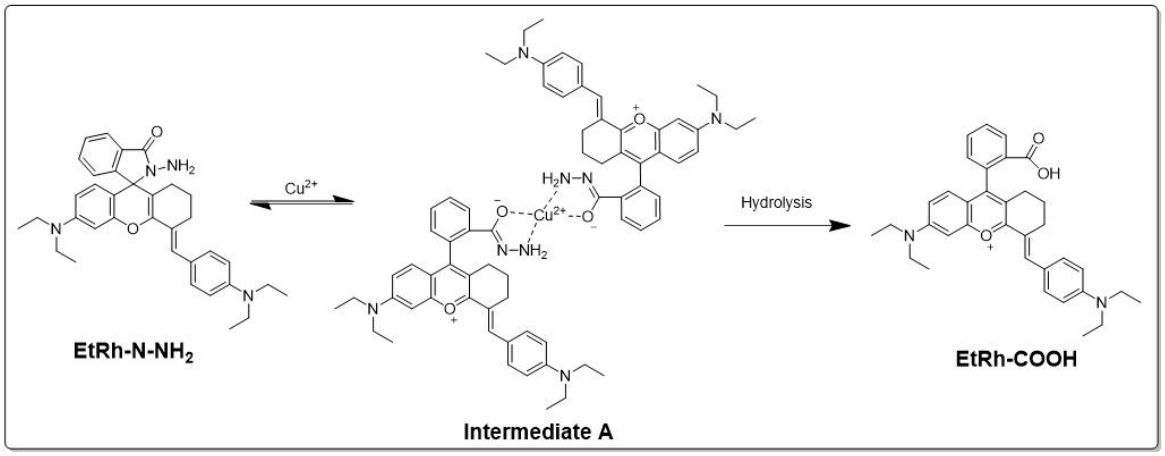

Scheme 3. Proposal of the mechanism for the fluorescent turning-on process.

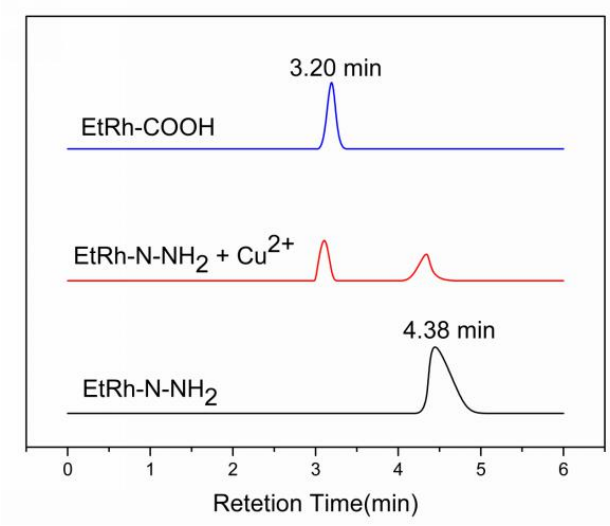

Fig. 1. HPLC chromatograms of EtRh-COOH (Blue), probe EtRh-N-NH_2 + Cu(II) (Red), EtRh-N-NH_2 (Black). Mobile phase: MeOH/EtCN (Gradient of 1/1 to 1/4, *v*/*v*).

2.3 Optical properties of EtRh-COOH and EtRh-N-NH_2

The absorbance spectra of **EtRh-N-NH_2** (in PBS) shows a clear peak at approximately 350 nm, and emission intensity of **EtRh-N-NH_2** from 690 nm to 900 nm is very weak. Besides, the solution is colorless; however, it turned blue after adding Cu(II). The 350 nm absorption peak decreased but a new band near 687 nm appeared and enhanced (Fig. 2A); meanwhile, a new band arose at 762 nm in the emission spectra (Fig. 2B). When the addition of Cu(II) with different concentrations (0–40 μM) is added to the probe(10 μM), the UV absorption of the probe at 687 nm and the fluorescence intensity at 762 nm gradually increase with the increase of Cu(II) concentration (Fig. 2C,D). The addition of 30 μM of Cu(II) triggered 235 fold enhancement of emission intensity in the range of 600–900 nm in 25 minutes (**Supplementary Fig. 2**). And in the range of 0–1.0 μM, the fluorescence emission intensity of the probe **EtRh-N-NH_2** at 762 nm shows a good linear relationship ($R^2 > 0.99$) with a detection limit (LOD) of 6 nM (LOD = 3 δ/k), displaying a very good sensitivity (Fig. 2E). The results manifest that the quantification of Cu(II) concentration can be achieved by utilizing the fluorescent spectral change behavior of **EtRh-N-NH_2** on Cu(II).

2.4 Influence of pH and temperature to the response

The effect of pH on the fluorescent change of probe **EtRh-N-NH_2** on Cu(II) was studied (Fig. 3A). It was shown that the fluorescence spectrum of the **EtRh-N-NH_2** solution remained unchanged at the pH range of 2.0 to 12.0 in the absence of Cu(II), which also indicated the excellent stability of the probe **EtRh-N-NH_2** in PBS solution. However, after the addition of Cu(II) (30 μM), a significant increase of the fluorescence intensity was observed

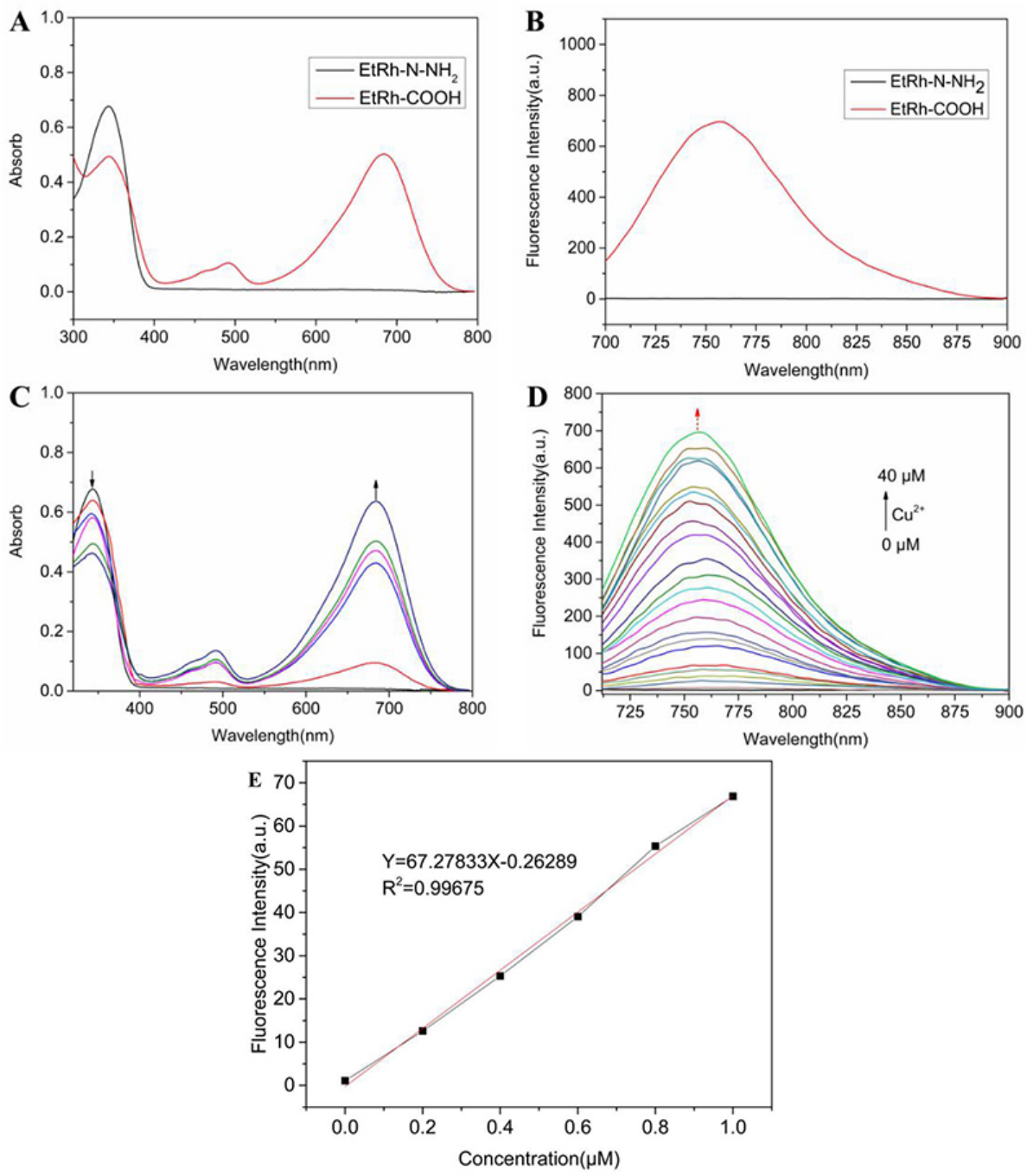

Fig. 2. Spectrum studies of the probe EtRh-N-NH$_2$. (A) The absorption spectrum of probe **EtRh-N-NH$_2$** and **EtRh-COOH** in PBS/EtOH (1/1, *v*/*v*). (B) The emission spectrum of probe **EtRh-N-NH$_2$** and **EtRh-COOH** in PBS/EtOH (1/1, *v*/*v*). (C) The absorption spectrum of **EtRh-N-NH$_2$** (10 μM) with Cu(II) in PBS/EtOH (1/1, *v*/*v*). (D) Fluorescence spectrum of **EtRh-N-NH$_2$** (10 μM) with Cu(II) in PBS/EtOH (1/1, *v*/*v*). (E) The fluorescence intensity increasement of **EtRh-N-NH$_2$** in the range of 0–1.0 μM.

when the pH was in the range from 6.0 to 8.0, and the increasement was almost equal within the range, but relative fewer increase was achieved was when pH was less than 6.0 or greater than 8.0. When the pH is below 4 or above 12, the response became relatively weak, presumably due to the reduced chemical reaction activity between Cu(II) and spirocyclic hydrazide group in the probe structure under strong acidic or basic environment. Meanwhile, the temperature effect of the fluorescent response was also investigated (Fig. 3B). The experiment data showed that the response efficiency was almost the same in the range of 25–50 °C. Therefore, the probe **EtRh-N-NH$_2$** can be used in both physiological pH (6.0–8.0) and temperature (37 °C).

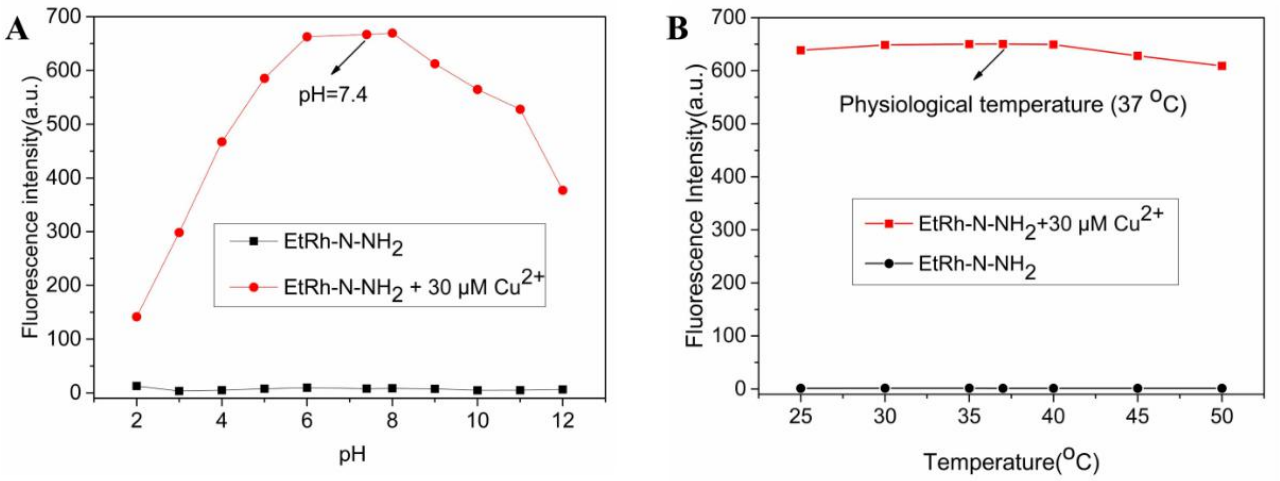

Fig. 3. The investigation of the influence of pH and temperature to the response. (A) Fluorescence response of 10 μM **EtRh-N-NH$_2$** in the pH range of 2.0–12.0 (black line) with 30 μM of Cu(II) (red line). (B) Fluorescence response under different temperature conditions (25–40 °C) of 10 μM **EtRh-N-NH$_2$** (black line) in the presence of 30 μM Cu(II) (red line). In the pH and temperature experiment, the probes are tested after incubating with Cu(II) for more than 30 minutes (λ_{ex} = 690 nm).

2.5 Selectivity studies

The selectivity of the probe over Cu(II) was examined to check if the probe can be employed in complex biochemical environment. Firstly, the solution of the probe **EtRh-N-NH$_2$** was treated with several common metal cations, including Al^{3+}, Ba^{2+}, Ca^{2+}, Co^{2+}, K^{+}, Mg^{2+}, Mn^{2+}, Na^{+}, Pb^{2+}, Zn^{2+}, Cd^{2+}, Hg^{2+}, Fe^{3+}, Fe^{2+}, $Ni^{2+}$and the mixture of all metal ions. The results suggested that only little enhancement was achieved in both absorbance and fluorescence spectrum (Fig. 4A,B), and the enhancements of these ions were insignificant comparing to that of Cu(II), demonstrating the superior selectivity of the probe **EtRh-N-NH$_2$** upon Cu(II) over other metals.

Human serum albumin (HSA) is the most abundant serum protein in the blood and can be used as a carrier for a variety of cargo molecules. Its apparent affinity for divalent copper has always been a concern, and it is considered to be the main Cu(II) binding ligand in blood and cerebrospinal fluid. We tested the binding ability of the probe to Cu(II) in the presence of different concentrations of HAS (Fig. 4C). The results proved that the affinity between HSA and Cu(II) was much high than the affinity between **EtRh-N-NH$_2$** and Cu(II). Moreover, considering that the Cu(II) can participate in the intracellular redox reaction, we conducted the control experiments with different reducing and oxidizing reagents (Fig. 4D). GSH can function as a reducing reagent intracellularly and turn Cu(II) into Cu(I). And when both Cu(II) and excessive GSH was added, negligible fluorescence was generated, demonstrating that Cu(I) was not responsive over the probe. Besides, when the reactive oxidizing species (H_2O_2 and ClO^{-}) were reacted with the probe, little fluorescence was formed, proving that the probe was nonreactive with by ROS.

In view of the above HSA and GSH responsive results, and considering the high content of HSA in the organism and GSH in the cells, the imaging of Cu(II) in living cells with the probe **EtRh-N-NH$_2$** would be indirect. Therefore, probes with less interference by HSA and GSH are needed to develop for the direct imaging of Cu(II) in living cells.

3. Experimental section

3.1 Reagents and instruments

The chemical reagents used are commercially available and purchased from J&K or Innochem chemical reagents. Commonly used solvents and chemical raw materials were all at analytically pure standard, and they were used without purification. The ^{1}H NMR and ^{13}C NMR spectrum were performed on a nuclear magnetic resonance spectrometer 400 (ASCEndTM400 (AVANCE HD III) with tetramethylsilane (TMS) as the internal standard. The high-resolution mass spectrum were tested on the American thermoelectric orbital ion trap mass spectrometer (LTQ-Orbitrap). The high-performance liquid chromatography was measured on the Agilent 1260 Infinity high performance liquid chromatograph. The ultraviolet were measured on the LS-45/55 fluorescence spectrophotometer (PerkinElmer, USA), and the fluorescence spectrum were measured on the UV-3200 ultraviolet-visible spectrophotometer.

3.2 Synthesis and characterization

3.2.1 Synthesis of Compound 2

Compound 2 was synthesized according to the method previously reported by our group [39]. Under ice bath conditions, 3 g of raw material 2-(4-diethylamino-2-hydro-xybenzoyl) benzoic acid (9.6 mmol) and 1.98 mL

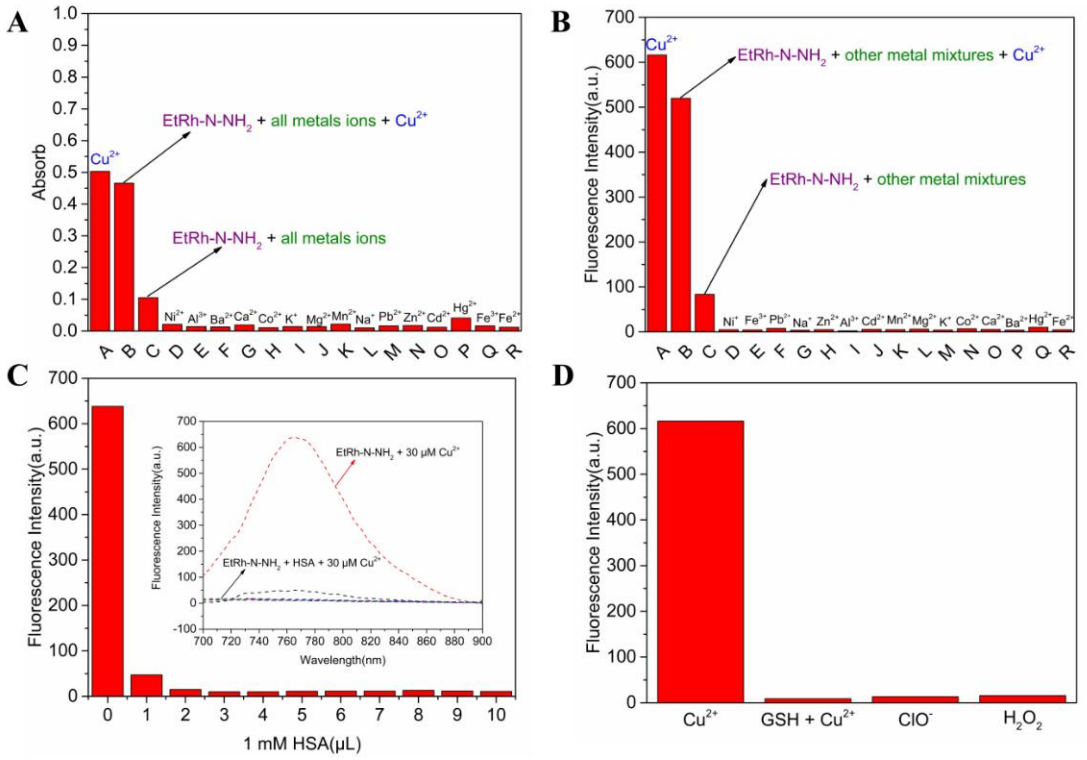

Fig. 4. Selectivity studies. (A) The UV-vis absorption and (B) fluorescent intensity (λ_{ex} = 690 nm) spectrum change of 10.0 μM **EtRh-N-NH$_2$** with 30 μM of Cu(II), and 100 μM of other cations (Al^{3+}, Ba^{2+}, Ca^{2+}, Co^{2+}, K^{+}, Mg^{2+}, Mn^{2+}, Na^{+}, Pb^{2+}, Zn^{2+}, Cd^{2+}, Hg^{2+}, Fe^{3+}, Fe^{2+}, Ni^{2+} and Cu(II)) in PBS/EtOH (1/1, *v*/*v*) solution (pH = 7.4), respectively. (C) Fluorescent intensity (λ_{ex} = 690 nm) spectrum change of 10.0 μM **EtRh-N-NH$_2$** with 1 mM HAS (0–10 μL) and 30 μM Cu(II). (D) Fluorescent intensity (λ_{ex} = 690 nm) spectrum change of 10.0 μM **EtRh-N-NH$_2$** with 100 μM GSH + 30 μM Cu(II), 100 μM H_2O_2, 100 μM ClO^{-} and 30 μM Cu(II) in PBS/EtOH (1/1, *v*/*v*) solution (pH = 7.4), respectively. In the selective experiment, the time of incubation with probe is more than 30 minutes.

cyclohexanone (19.2 mmol) were placed in a 15 mL round bottle, and the resulting mixture was heated at 90 °C for 2 hours. After the reaction was completed (monitored by TLC), the reaction mixture was cooled to room temperature and poured into ice water. Then, 2 mL of perchloric acid was added and stirred until a large amount of precipitation was generated. The **Compound 2** was obtained as red solid after filtration (3.6 g, 79% yield), mp: 82.8 °C. IR (KBr, cm^{-1}): 3435, *v* (O-H); 2934, *v* (C-H); 1716, 1640, *v* (C = O); 1462, *v* (C-N); 1324, *v* (C-O); 1270, *v* (Ar-O); ^{1}H NMR (400 MHz, $CDCl_3$) δ 8.26 (d, *J* = 7.8 Hz, 1H), 7.77 (td, *J* = 7.5, 0.9 Hz, 1H), 7.66 (dd, *J* = 11.2, 4.2 Hz, 1H), 7.21 (d, *J* = 7.3 Hz, 1H), 7.06 (s, 2H), 6.86 (s, 1H), 3.62 (q, *J* = 7.2 Hz, 4H), 3.09 (m, 2H), 2.25 (m, 2H), 2.01–1.90 (m, 2H), 1.75 (m, 2H), 1.30 (t, *J* = 6.8 Hz, 6H) (**Supplementary Fig. 3**). ^{13}C NMR (100 MHz, $CDCl_3$, ppm) δ 170.12, 166.83, 165.11, 159.51, 155.72, 134.39, 133.50, 131.79, 130.29, 129.27–128.88, 128.71, 121.81, 118.07, 117.49, 95.49, 46.25, 29.53, 25.06, 21.33, 20.89, 12.50 (**Supplementary Fig. 4**). HRMS (ESI): m/z calcd for $C_{24}H_{26}NO_3^{+}$ $[M]^{+}$: 376.1907, found: 376.1907 (**Supplementary Fig. 5**).

3.2.2 Synthesis of EtRh-COOH

4-Diethylaminobenzaldehyde (0.13 g, 0.76 mmol) was added to a solution of **Compound 2** (0.3 g, 0.63 mmol) in 10 mL of glacial acetic acid, and the resulting mixture was heated at 100 °C for 6 h. Acetic acid was removed by rotary vapor, and the residue was purified by column chromatography on silica gel with dichloromethane and methanol (100/1 to 50/1, *v*/*v*) as eluent. **Compound EtRh-COOH** was afforded as a blue solid (213 mg, 63% yield), mp: 117.5–119.1 °C. IR (KBr, cm^{-1}): 2964, 2924, 2854, *v* (C-H); 1714, *v* (C = O); 1314, *v* (C-O); 1258, *v* (Ar-O); 1126, 1064, *v* (C-N); ^{1}H NMR (400 MHz, DMSO-d_6, ppm) δ 13.26 (s, 1H), 8.15 (d, *J* = 7.7 Hz, 1H), 8.03 (s, 1H), 7.84 (td, *J* = 7.5, 1.0 Hz, 1H), 7.74 (dd, *J* = 11.4, 3.8 Hz, 1H), 7.60 (d, *J* = 8.6 Hz, 2H), 7.36 (d, *J* = 7.4 Hz, 1H), 7.15 (s, 1H), 7.02 (s, 1H), 6.81 (t, *J* = 11.3 Hz, 3H), 3.63–3.53 (m, 4H), 3.47 (dd, *J* = 13.9, 6.9 Hz, 4H), 2.89 (d, *J* = 5.3 Hz, 2H), 2.18 (s, 2H), 1.81–1.63 (m, 2H), 1.20 (t, *J* = 7.0 Hz, 6H), 1.15 (t, *J* = 7.0 Hz, 6H) (**Supplementary Fig. 6**). ^{13}C NMR (100 MHz, $CDCl_3$, ppm) δ 166.98, 157.65, 154.47, 150.08, 135.25, 133.55, 131.29, 130.49, 130.22, 129.44, 123.06, 122.24, 116.74,

112.07, 96.08, 55.38, 49.07, 45.51, 44.54, 27.46, 25.95, 21.36, 12.99 (**Supplementary Fig. 7**). HRMS (ESI): m/z calcd for $C_{35}H_{39}N_2O_3^+$ $[M]^+$: 535.2955, found: 535.2955 (**Supplementary Fig. 8**).

3.2.3 Synthesis of EtRh-N-NH_2

Hydrazine hydrate (1.9 mmol) and PyBOP (0.09 g, 0.19 mmol) were added to a solution of **EtRh-COOH** (0.1 g, 0.19 mmol) in dry dichloromethane. The mixture was vigorously stirred at ambient temperature (~20 °C) for 3 hours. Then the dichloromethane was removed with rotary vapor. The residue was purified by column chromatography on silica gel using ethyl acetate and petroleum ether (*v*/*v*, 5/0 to 5/1) as the eluent to obtain compound **EtRh-N-NH_2** as a yellow solid (43 mg, 41% yield), mp: 169.6–170.4 °C. IR (KBr, cm^{-1}): 3435, 1517, *v* (N-H); 2968, 2928, *v* (C-H); 1606, *v* (C = O); 1355, 1375, 1466, *v* (C-N); 1267, *v* (Ar-O). ^{1}H NMR (400 MHz, $CDCl_3$, ppm) δ 7.92 (d, J = 7.3 Hz, 1H), 7.52 (t, J = 7.2 Hz, 1H), 7.47 (t, J = 7.2 Hz, 1H), 7.33 (d, J = 8.7 Hz, 2H), 7.23 (d, J = 7.3 Hz, 1H), 6.70 (d, J = 8.7 Hz, 2H), 6.44 (d, J = 2.2 Hz, 1H), 6.37 (d, J = 8.8 Hz, 1H), 6.30 (dd, J = 8.8, 2.2 Hz, 1H), 3.71 (s, 2H), 3.51 (s, 1H), 3.41 (dd, J = 12.5, 5.5 Hz, 4H), 3.36 (dd, J = 12.5, 5.5 Hz, 4H), 2.79 (d, J = 29.0 Hz, 2H), 1.76 (dt, J = 10.6, 4.8 Hz, 1H), 1.64–1.48 (m, 3H), 1.22 (d, J = 7.1 Hz, 6H), 1.18 (d, J = 7.1 Hz, 6H) (**Supplementary Fig. 9**). ^{13}C NMR (100 MHz, $CDCl_3$, ppm) δ 166.39, 153.19, 149.52, 148.77, 148.02, 146.59, 132.41, 130.98, 128.33, 127.64, 126.63, 124.39, 123.49, 123.03, 111.12, 108.35, 105.56, 103.63, 97.93, 67.69, 44.35, 27.72, 22.79, 12.67 (**Supplementary Fig. 10**). HRMS (ESI): m/z calcd for $C_{35}H_{41}N_4O_2^+$ $[M + H]^+$: 549.3230, found: 549.3228 (**Supplementary Fig. 11**).

4. Conclusions

In conclusion, we developed a rhodamine derivative **EtRh-N-NH_2** as a fluorescent probe for the detection of Cu(II). The Cu(II) compounds were successfully recognized by the hydrazine moiety, releasing the product **EtRh-COOH** with high fluorescence and producing the fluorescence signal. The recognition was sensitive, specific, and rapid. The detection limit is only 6 nM. The product **EtRh-COOH** exhibited a NIR region of emission wavelength at 762 nm, and its Stokes shift is as large as 75 nm. The development of probes with the ability of Cu(II) imaging in living cells is underway.

Abbreviations

NIR, near-infrared; ICP, inductively coupled plasma; AAS, atomic absorption spectroscopy; AES, atomic emission spectroscopy; MS, mass spectrometry; PET, photoinduced electron transfer; MeOH, methanol; EtCN, acetonitrile; PBS, phosphate buffer saline; UV, ultravioletradiation; LOD, limit of detection; EtOH, ethanol; LSCM, laser scanning confocal microscope; NMR, nuclear magnetic resonance; TMS, tetramethylsilane; TLC, thin layer chromatography; IR, infrared radiation; DMSO, Dimethyl sulfoxide.

Author contributions

LH, YL, HZ and SM designed the study. YL, PW and ML designed and performed the experiments. LH, YL, PW, ML and SM analyzed the data. YL and SM wrote the paper.

Ethics approval and consent to participate

Not applicable.

Acknowledgment

Thanks to all the peer reviewers for their opinions and suggestions.

Funding

The authors would like to acknowledge financial support from Beijing Key Laboratory of Environmental & Viral Oncology, Beijing Key Laboratory for Green Catalysis and Separation, Beijing Postdoctoral Research Foundation (No. 2020-ZZ-028), Postdoctoral Research Foundation of Beijing Chaoyang district (No. 2020-ZZ-027).

Conflict of interest

The authors declare no conflict of interest.

Supplementary material

Supplementary material associated with this article can be found, in the online version, at https://www.imrpress.com/journal/FBL/27/1/10.31083/j.fbl2701028.

References

[1] Gaier ED, Eipper BA, Mains RE. Copper signaling in the mammalian nervous system: synaptic effects. Journal of Neuroscience Research. 2013; 91: 2–19.

[2] Peng B, Fan M, Xu J, Guo Y, Ma Y, Zhou M, *et al*. Dual-emission ratio fluorescent probes based on carbon dots and gold nanoclusters for visual and fluorescent detection of copper ions. Microchimica Acta. 2020; 187: 660.

[3] He G, Liu C, Liu X, Wang Q, Fan A, Wang S, *et al*. Design and synthesis of a fluorescent probe based on naphthalene anhydride and its detection of copper ions. PLoS ONE. 2017; 12: e0186994.

[4] Behbahani M, Abolhasani J, Amini MM, Sadeghi O, Omidi F, Bagheri A, *et al*. Application of mercapto ordered carbohydrate-derived porous carbons for trace detection of cadmium and copper ions in agricultural products. Food Chemistry. 2015; 173: 1207–1212.

[5] Gaggelli E, Kozlowski H, Valensin D, Valensin G. Copper homeostasis and neurodegenerative disorders (Alzheimer's, prion, and Parkinson's diseases and amyotrophic lateral sclerosis). Chemical Reviews. 2006; 106: 1995–2044.

[6] Desai V, Kaler SG. Role of copper in human neurological disorders. American Journal of Clinical Nutrition. 2008; 88: 855S–858S.

[7] Gonzáles APS, Firmino MA, Nomura CS, Rocha FRP, Oliveira PV, Gaubeur I. Peat as a natural solid-phase for copper pre-

concentration and determination in a multicommuted flow system coupled to flame atomic absorption spectrometry. Analytica Chimica Acta. 2009; 636: 198–204.
[8] Zaksas NP, Gerasimov VA, Nevinsky GA. Simultaneous determination of Fe, P, Ca, Mg, Zn, and Cu in whole blood by two-jet plasma atomic emission spectrometry. Talanta. 2010; 80: 2187–2190.
[9] Liu Y, Liang P, Guo L. Nanometer titanium dioxide immobilized on silica gel as sorbent for preconcentration of metal ions prior to their determination by inductively coupled plasma atomic emission spectrometry. Talanta. 2005; 68: 25–30.
[10] Huang X, Li Z, Liu Z, Zeng C, Hu L. A near-infrared fluorescent probe for endogenous hydrogen peroxide real-time imaging in living cells and zebrafish. Dyes and Pigments. 2019; 165: 518–523.
[11] Mehta VN, Desai ML, Basu H, Kumar Singhal R, Kailasa SK. Recent developments on fluorescent hybrid nanomaterials for metal ions sensing and bioimaging applications: a review. Journal of Molecular Liquids. 2021; 333: 115950.
[12] Sharma S, Ghosh KS. Recent advances (2017–20) in the detection of copper ion by using fluorescence sensors working through transfer of photo-induced electron (PET), excited-state intramolecular proton (ESIPT) and Förster resonance energy (FRET). Spectrochimica Acta Part A: Molecular and Biomolecular Spectroscopy. 2021; 254: 119610.
[13] Ruedas-Rama MJ, Walters JD, Orte A, Hall EAH. Fluorescent nanoparticles for intracellular sensing: a review. Analytica Chimica Acta. 2012; 751: 1–23.
[14] Liu ML, Chen BB, Li CM, Huang CZ. Carbon dots: synthesis, formation mechanism, fluorescence origin and sensing applications. Green Chemistry. 2019; 21: 449–471.
[15] Lake RJ, Yang Z, Zhang J, Lu Y. DNAzymes as Activity-Based Sensors for Metal Ions: Recent Applications, Demonstrated Advantages, Current Challenges, and Future Directions. Accounts of Chemical Research. 2019; 52: 3275–3286.
[16] Xu W, Ren C, Teoh CL, Peng J, Gadre SH, Rhee H, *et al*. An artificial tongue fluorescent sensor array for identification and quantitation of various heavy metal ions. Analytical Chemistry. 2014; 86: 8763–8769.
[17] Zhang J, Zhu M, Jiang D, Zhang H, Li L, Zhang G, *et al*. A FRET-based colorimetric and ratiometric fluorescent probe for the detection of Cu2+ with a new trimethylindolin fluorophore. New Journal of Chemistry. 2019; 43: 10176–10182.
[18] Bagheri M, Masoomi MY. Sensitive Ratiometric Fluorescent Metal-Organic Framework Sensor for Calcium Signaling in Human Blood Ionic Concentration Media. ACS Applied Materials & Interfaces. 2020; 12: 4625–4631.
[19] Lin Z, Xue S, Chen Z, Han X, Shi G, Zhang M. Bioinspired Copolymers Based Nose/Tongue-Mimic Chemosensor for Label-Free Fluorescent Pattern Discrimination of Metal Ions in Biofluids. Analytical Chemistry. 2018; 90: 8248–8253.
[20] Qu W, Yan G, Ma X, Wei T, Lin Q, Yao H, *et al*. "Cascade recognition" of Cu2+ and H2PO4− with high sensitivity and selectivity in aqueous media based on the effect of ESIPT. Sensors and Actuators B: Chemical. 2017; 242: 849–856.
[21] Peng J, Li J, Xu W, Wang L, Su D, Teoh CL, *et al*. Silica Nanoparticle-Enhanced Fluorescent Sensor Array for Heavy Metal Ions Detection in Colloid Solution. Analytical Chemistry. 2018; 90: 1628–1634.
[22] Yang Y, Zhao Q, Feng W, Li F. Luminescent chemodosimeters for bioimaging. Chemical Reviews. 2013; 113: 192–270.
[23] Zhou Z, Tang H, Chen S, Huang Y, Zhu X, Li H, *et al*. A turn-on red-emitting fluorescent probe for determination of copper(II) ions in food samples and living zebrafish. Food Chemistry. 2021; 343: 128513.
[24] Ramdass A, Sathish V, Babu E, Velayudham M, Thanasekaran P, Rajagopal S. Recent developments on optical and electrochemical sensing of copper(II) ion based on transition metal complexes. Coordination Chemistry Reviews. 2017; 343: 278–307.
[25] Yang Y, Zhao Q, Feng W, Li F. Luminescent chemodosimeters for bioimaging. Chemical Reviews. 2013; 113: 192–270.
[26] Ni H, Wang Q, Jin L, Wang W, Dai L, Zhao C. High selectivity and reversibility/reusability red emitting fluorescent probe for copper ions detection and imaging in living cells. Journal of Luminescence. 2019; 206: 125–131.
[27] Saleem M, Rafiq M, Hanif M, Shaheen MA, Seo S. A Brief Review on Fluorescent Copper Sensor Based on Conjugated Organic Dyes. Journal of Fluorescence. 2018; 28: 97–165.
[28] Li H, Guo Y, Lei Y, Gao W, Liu M, Chen J, *et al*. D-p-A benzo[c][1,2,5] selenadiazole-based derivatives via an ethynyl bridge: photophysical properties, solvatochromism and applicationsas fluorescent sensors. Dyes and Pigments. 2015; 112: 105–115.
[29] Cotruvo JA, Aron AT, Ramos-Torres KM, Chang CJ. Synthetic fluorescent probes for studying copper in biological systems. Chemical Society Reviews. 2016; 44: 4400–4414.
[30] Liu Y, Sun Y, Du J, Lv X, Zhao Y, Chen M, *et al*. Highly sensitive and selective turn-on fluorescent and chromogenic probe for Cu(II) and ClO- based on a N-picolinyl rhodamine B-hydrazide derivative. Organic & Biomolecular Chemistry. 2011; 9: 432–437.
[31] Liu K, Shang H, Meng F, Liu Y, Lin W. A novel near-infrared fluorescent platform with good photostability and the application for a reaction-based Cu(II) probe in living cells. Talanta. 2016; 147:193–198.
[32] Wechakorn K, Prabpai S, Suksen K, Kanjanasirirat P, Pewkliang Y, Borwornpinyo S, *et al*. A rhodamine-triazole fluorescent chemodosimeter for Cu(II) detection and its application in bioimaging. Luminescence. 2018; 33: 64–70.
[33] Mo S, Zhang X, Hameed S, Zhou Y, Dai Z. Glutathione-responsive disassembly of disulfide dicyanine for tumor imaging with reduction in background signal intensity. Theranostics. 2020; 10: 2130–2140.
[34] Qian X, Xu Z. Fluorescence imaging of metal ions implicated in diseases. Chemical Society Reviews. 2016; 44: 4487–4493.
[35] Li Z, Wang Y, Zeng C, Hu L, Liang X. Ultrasensitive Tyrosinase-Activated Turn-on near-Infrared Fluorescent Probe with a Rationally Designed Urea Bond for Selective Imaging and Photodamage to Melanoma Cells. Analytical Chemistry. 2018; 90: 3666–3669.
[36] Wang X, Zhang L, Li Q, Gao Y. A novel dark resonance energy transfer-based fluorescent probe with large Stokes shift for the detection of pH and its imaging application. Dyes and Pigments. 2020; 181: 108614.
[37] Saleem M, Lee K. Selective fluorescence detection of Cu2+ in aqueous solution and living cells. Journal of Luminescence. 2014; 145: 843–848.
[38] Wang J, Li H, Long L, Xiao G, Xie D. Fast responsive fluorescence turn-on sensor for Cu2+ and its application in live cell imaging. Journal of Luminescence. 2012; 132: 2456–2461.
[39] Gu T, Mo S, Mu Y, Huang X, Hu L. Detection of endogenous hydrogen peroxide in living cells with para-nitrophenyl oxoacetyl rhodamine as turn-on mitochondria-targeted fluorescent probe. Sensors and Actuators B: Chemical. 2020; 309: 127731.